This is a preprint, the final version is subject to change, of the American Mineralogist (MSA)
Cite as Authors (Year) Title. American Mineralogist, in press.
DOI: https://doi.org/10.2138/am-2020-7360

Revision 2

Regular article

Crystal structure and Raman spectroscopic studies of OH stretching vibrations in Zn-rich fluor-elbaite

Raman spectroscopic studies of OH stretching vibrations in Zn-rich fluor-ebaite

ADAM PIECZKA[1*], ANDREAS ERTL[2], BOŻENA GOŁĘBIOWSKA[1], PIOTR JELEŃ[3], JAKUB KOTOWSKI[4], KRZYSZTOF NEJBERT[4], MARCIN STACHOWICZ[4] AND GERALD GIESTER[2]

[1] Department of Mineralogy, Petrography and Geochemistry, AGH University of Science and Technology, Mickiewicza 30, 30-059 Kraków, Poland

[2] Institut für Mineralogie und Kristallographie, Geozentrum, Universität Wien, Althanstrasse 14, 1090 Wien, Austria

[3] Faculty of Materials Science and Ceramics, AGH University of Science and Technology, Mickiewicza 30, 30-059 Kraków, Poland

[4] University of Warsaw, Faculty of Geology, Institute of Geochemistry, Mineralogy and Petrology, 02-089 Warszawa, Żwirki and Wigury 93, Poland

**corresponding author*: pieczka@agh.edu.pl

ABSTRACT

Zinc-rich fluor-elbaite from Piława Górna, Poland, was studied by electron microprobe (EPMA), single-crystal X-ray diffraction (SREF) and Raman spectroscopy (RS) to check the possibility of an application of RS, to draw crystal chemical conclusions for Al-rich and Li-bearing tourmalines on basis of the O–H stretching vibrations in the spectral range 3400–3800 cm^{-1}. This tourmaline, forming a thin metasomatic zone around gahnite, features varying compositions with a ZnO content reaching in the studied fragment of 5.70(12) wt%. The crystal structure of this Zn-rich fluor-elbaite [a = 15.921(1), c = 7.127(1) Å] was refined with a $R1$ value of 1.67 %. Its formula was determined on the basis of electron-microprobe and structure refinement as $^{X}(Na_{0.84}\square_{0.14}Ca_{0.01})_{\Sigma 1.00}{}^{Y}(Al_{1.06}Li_{0.84}Zn_{0.69}Fe^{2+}_{0.32}Mn_{0.09})_{\Sigma 3.00}{}^{Z}Al_6(BO_3)_3(^{T}Si_6O_{18})^{V}(OH)_3{}^{W}(F_{0.65}OH_{0.26}O_{0.09})$. The deconvolution of the O–H stretching vibration bands, performed by fitting of an input model of component bands with Gaussian function shapes for the empirical spectrum, indicates that each of the three maxima assigned for ^{V}OH bonded to $^{Y}Al^{3+}$, Y^{2+}, and $^{Y}Li^{+}$ and with the total integral intensity of at least 75% of the total OH content could be resolved into 1 to 3 bands, depending on the X-site occupation (vacancies, Na^{+} and Ca^{2+}). The deconvolution indicates further that several low intense bands of $^{W}O–H$ modes above a Raman shift of 3600 cm^{-1}, totally reaching ≤25 %, are dependent on the occupation of triplets of YYY cations bonded to the hydroxyl. These $^{W}O–H$ modes are also influenced by the X-site occupation. Due to ordering of all octahedral cations (except Al) at the Y site and a complete occupation of the Z site by Al and the V site by OH, it seems possible to evaluate the Li and OH contents in a Al-rich and Li-bearing tourmaline directly from the Raman spectrum. By using the ratio $^{V}OH_{I_{Y}Al^{Z}Al^{Z}Al}$ / ($^{V}OH_{I_{YZZ}} + {}^{W}OH_{I_{YYY}}$) as evaluated from RS, corresponding to the ratio ^{Y}Al / ^{V+W}OH in the crystal, the formula of the Zn-bearing fluor-elbaite can be calculated as $^{X}(Na_{0.85}\square_{0.14}Ca_{0.01})_{\Sigma 1.00}{}^{Y}(Al_{1.11}Y^{2+}_{1.11}Li_{0.78})_{\Sigma 3.00}{}^{Z}Al_6(BO_3)_3(Si_6O_{18})(OH)_3(F_{0.65}OH_{0.13}O_{0.22})$, where

Y^{2+} = Zn + Fe + Mn. The formula, determined only on basis of EPMA and deconvolution of RS in the O–H stretching bands, corresponds very well (≤1 sd range of EPMA) to the formula determined on basis of EPMA and SREF. This result implicates that the O–H stretching vibrations, measured by Raman spectroscopy, can by applied for Al-rich and Li-bearing tourmalines as a useful tool for an additional information for determining the crystal chemical formula. It is also very helpful when crystal structural data are not available.

Key-words: Zn-rich fluor-elbaite, structure refinement, Raman spectroscopy, OH stretching vibrations, lithium content, hydroxyl content.

INTRODUCTION

The tourmaline supergroup comprises complex borosilicates that are found as accessory minerals in a wide variety of igneous, metamorphic and sedimentary rocks due to their stability over a wide range in pressure, temperature and composition (Van Hinsberg et al. 2011). The generalized formula of tourmaline-supergroup minerals is $XY_3Z_6(T_6O_{18})(BO_3)_3V_3W$, where X, Y, Z, T, B, V (=O3) and W (=O1) denote different structural sites (Henry et al. 2011). These sites can have different possible occupants:

^{IX}X – Na^+, K^+, Ca^{2+}, Pb^{2+}, □ (vacancy),

^{VI}Y – Fe^{2+}, Mg^{2+}, Mn^{2+}, Al^{3+}, Li^+, Fe^{3+}, Cr^{3+}, V^{3+}, Ti^{4+}, Zn^{2+}, Cu^{2+}, Ni^{2+}, ...

^{VI}Z – Al^{3+}, Fe^{3+}, Cr^{3+}, V^{3+}, Mg^{2+}, Fe^{2+}, ...

^{IV}T – Si^{4+}, Al^{3+}, B^{3+},

^{III}B – B^{3+},

^{III}V – OH^-, O^{2-},

^{III}W – OH^-, F^-, O^{2-}

Some of these constituents can be simultaneously present on two and even three structural sites, reflecting order-disorder phenomenon mainly between the octahedral Y- and Z-site occupants or oxygen and hydroxyl on the V and W sites. Substitutions among the heterovalent Y- and Z-site occupants are often coupled with ion replacements at other structural sites, mainly at the X, V and W. Four of the sites (Y, Z, V, W) form an octahedral cluster [$V_3Y_3Z_6W$] developed in the unit cell around (0, 0, 0), (2/3, 1/3/, 1/3) and (1/3, 2/3, 2/3), with a symmetry consistent with the *R*3*m* space group. In consequence of these substitutions, the tourmaline supergroup comprises currently 35 valid mineral species accepted by the Commission on New Minerals, Nomenclature and Classification (CNMNC) of the International Mineralogical Association (IMA). They represent hydroxyl-, fluor- and oxy-species of X-vacant-, alkali- and calcic tourmalines with typical octahedral occupants like Fe^{2+}, Mg^{2+}, Mn^{2+}, Al^{3+}, Li^{+}, Fe^{3+}, Cr^{3+} and V^{3+} (Henry et al. 2011). Much less common are crystals highly enriched in atypical components like Pb (Sokolov and Martin 2009), Ti (Lottermoser and Plimer 1987; Vezzoni et al. 2018), Cu (Vereshchagin et al. 2013), Ni (Baksheev and Kudryavtseva 2004), Mn^{3+} (Bosi et al. 2017), Zn (Sokolov et al. 1988; Henry and Dutrow 1996; Ferreira et al. 2005; Pieczka et al. 2018), or K (Žáček et al. 2000; Lussier et al. 2016). The Zn-enriched tourmalines are represented mainly by fluor-elbaite, rarer elbaite, in which Zn^{2+}, beside typical Al^{3+} and Li^{+}, is one of the main octahedral Y-site occupants. Until quite lately, the most Zn-enriched tourmaline (3.83 wt% ZnO) was known from a rare-element-bearing pegmatite of Russia (Sokolov et al. 1988). However recently, Pieczka et al. (2018) described Zn-rich fluor-elbaite and elbaite containing up to 6.32 and 7.37 wt% ZnO, respectively, in a rare-element dyke of the Julianna pegmatitic system, exposed during mining works in a migmatite-amphibolite quarry at Piława Górna, Lower Silesia, Poland (Szuszkiewicz et al. 2013). In the dyke, these tourmalines, associated with Zn-enriched schorl and foitite (up to 2.45 wt% ZnO), formed a thin metasomatic zone around gahnite, changing progressively into

typical, only slightly Zn-enriched, fluor-elbaite and elbaite. In the original paper, the occurrence and compositional relationships of the tourmalines were described in detail, as well as a Raman spectrum of Zn-rich fluor-elbaite was presented. Unfortunately, in Pieczka et al. (2018) the captions for Figures 9a and 9b presenting the Raman spectra of O–H stretching modes in Zn-rich fluor-elbaite and associated (Zn,Li)-bearing schorl in the range of 3400–3800 cm^{-1} were inadvertently switched, i.e. the caption (b) should be (a) and conversely, consistent with Figure 8 presenting both these spectra in the range of 50–4000 cm^{-1}.

Raman spectroscopy is a method commonly used in mineralogy for a quick identification of minerals because an extensive sample preparation is not necessary and, similarly as infra-red spectroscopy, it is known as a non-destructive method giving fingerprint of a specific species. The great advantage of Raman spectroscopy is its capability to analyze areas as small as ~1 μm^2, which makes it useful in studies of highly heterogeneous materials, which require micrometer-scale spatial resolution. The acquisition area of the method is only somewhat smaller, but may be comparable with the acquisition area of the wave-length-dispersive electron probe microanalysis (EPMA-WDS), at least an order of magnitude smaller than the crystal dimensions required by single-crystal X-ray diffraction as the basic method of structure recognition. This capability can make Raman spectroscopy a very useful and complementary tool in crystal chemical and structural studies. Moreover, because ^{V}OH and ^{W}OH anions are bonded to different Y-site occupants as well as to Al at the Z site, O–H stretching modes in Raman spectra of Li-bearing tourmalines contain critical crystal-chemical and structural information of the structural part with the greatest compositional variation. Therefore, in this paper we analyze the possibility of a Raman spectroscopy application for a fast evaluation of crystal chemical relationships in Li-bearing tourmalines, especially the quantitative estimation of the Y-site population and of the ^{W}OH amount. To present the possibilities of Raman spectroscopy, we discuss the crystal structure

and explain in detail the Raman spectrum of this Zn-rich fluor-elbaite, especially focusing on O–H stretching vibrations in which our interpretation is in agreement with the structural and compositional results.

MATERIALS AND METHODS

Electron probe microanalysis (EPMA)

Electron probe microanalysis of Zn-rich fluor-elbaite in a zone around gahnite was performed at the Inter-Institute Analytical Complex for Minerals and Synthetic Substances at the University of Warsaw, Poland, using a Cameca SX 100 electron microprobe (CAMECA, Cedex, France). The analyses were made on a grinded, polished and coated with carbon small fragment of the pegmatite with the gahnite crystals overgrown by Zn-rich fluor-elbaite mounted in 1-inch epoxy disc. The microprobe operated in WDS mode under the following conditions: accelerating voltage of 15 kV, beam current of 10 nA, beam diameter of 2 μm, peak count-time of 20 s, background time of 10 s. Standards (analytical lines, diffracting crystals and mean detection limits in wt % element) were as follows: fluorophlogopite (F *K*α, PC0, 0.12), albite (Na *K*α, TAP, 0.03), diopside (Mg *K*α, TAP, 0.02), (Si *K*α, TAP, 0.03) and (Ca *K*α, PET, 0.02), orthoclase (Al *K*α, TAP, 0.03) and (K *K*α, PET, 0.02), rutile (Ti *K*α, LPET, 0.02), rhodonite (Mn *K*α, LIF, 0.09), hematite (Fe *K*α, LIF, 0.08), V_2O_5 (V *K*α, LIF, 0.06), Cr_2O_3 (Cr *K*α, LPET, 0.02), and sphalerite (Zn *K*α, LIF, 0.09). The raw data were reduced with the PAP routine of Pouchou and Pichoir (1991). The estimation of the Li_2O amounts from EPMA results on the basis of a multiple-regression equation of Pesquera et al. (2016) did not give positive result because the calculated Li_2O amount (in wt%) is distinctly ZnO dependent for higher ZnO contents (Pieczka et al. 2018). Therefore, we estimated the Li_2O and H_2O contents on the basis of the refined Y- and W-site scattering values. The atomic contents and chemical formula of the Zn-rich fluor-elbaite were

normalized in relation to 14.5 (O,OH,F) anions pfu, i.e. 31 (O,OH,F) – 12 O – 4.5 O after assumption the presence of 6 Si atoms per formula unit (apfu), 3 B apfu, total Fe as FeO, and Li_2O and H_2O amounts matching the calculated Li and OH contents during the formula calculation to the refined Y-site electron density, and the sum of Y-site occupants equal to 3 apfu. A small excess of Si above 6 apfu for the measured SiO_2 amount indicated at the applied normalization was considered as a small inaccuracy in the SiO_2 analysis [below 1.5 standard deviation (sd) of a single EPMA Si determination] or as an external admixture, e.g. of quartz micro-inclusions occurring in the Zn-rich fluor-elbaite zone. The EPMA results recalculated in such way presented in Table 1 correspond to spot analyses of Zn-rich fluor-elbaite, observed in one area of a zone around gahnite (Fig. 1). From this area, in which also micro-Raman spectra were collected (discussed in Pieczka et al. 2018), we extracted a small fragment of this tourmaline for the single-crystal X-ray diffraction investigation.

Crystal structure refinement (SREF)

The crystal structure of Zn-rich fluor-elbaite was refined at the Institut für Mineralogie und Kristallographie, Geozentrum, Universität Wien, Austria. As a first step, the quality of different tourmaline crystals was checked with a Bruker APEXII diffractometer equipped with a CCD area detector and an Incoatec Microfocus Source IμS (30 W, multilayer mirror, Mo*K*α). The crystal with the best quality, 170 × 150 × 120 μm in size, was subsequently measured on this diffractometer. Single-crystal X-ray diffraction data, up to 80.52° 2θ, were collected at room temperature, integrated and corrected for Lorentz and polarization factors with an absorption correction by evaluation of partial multiscans. The structure was refined with SHELXL97 (Sheldrick 1998) using scattering factors for neutral atoms and a tourmaline starting model from Ertl et al. (2010) (sample R6b). Refinement was performed with anisotropic displacement parameters for all non-hydrogen atoms. Supplemental Material (CIF file) provides crystal data

and details of the structure refinement. The various site occupancies were refined according to well-known characteristics of the tourmaline structure, and considering the electron-probe analysis; this strategy appears sound with the resulting empirical formula being compatible with that determined from the EPMA results. Hence, the X site occupancy was refined by using a Na scattering factor, the Y site with Zn and Li scattering factors, and the W site with F and O scattering factors, whereas the Si occupancy at the T site and the Al occupancy at the Z site were fixed at 1.00, typical for (Al,Li)-bearing tourmalines. A preliminary refinement, with O1 and O2 sites constrained to their positions of maximum site-symmetry, has shown relatively high U_{eq} values for these both oxygen sites. Following the findings of Burns et al. (1994), who reported high U_{eq} values for the O1 and O2 sites that indicate position disorder, the crystal structure was finally refined with both oxygen sites allowed to disorder with coordinates (x, x/2, z) and (x, y, z). The refinement converged at a *R*1(F) value of 1.67%.

Raman spectroscopy (RS)

Raman spectra of Zn-rich fluor-elbaite were collected in back-scattered geometry at the Faculty of Materials Science and Ceramics, AGH UST, Cracow, Poland, with a Horiba Labram HR spectrometer integrated with an Olympus BX 41 confocal microscope. The system was calibrated using the 520.7 cm^{-1} Raman band of Si. The spectra were recorded in the range of 50–4000 cm^{-1} using the 532 nm line of a solid-state Nd-YAG laser (10 mW) and 1800 grating, on randomly oriented surfaces of Zn-rich tourmaline in a fragment of the pegmatite mounted in epoxy resin that was used previously for EPMA and partly extracted for SREF studies. Prior to the Raman measurements the carbon coating of the disc was removed. The Raman measurements were carried out by accumulation of two scans with precision ± 0.39 cm^{-1}, each with an acquisition time of 600 s at the microscope magnification 100×; the minimum lateral and depth resolution ~1 μm, and an estimated analytical spot size of ~1 μm. Because all the spectra recorded on a small

fragment of the tourmaline were very similar one to the other in the range of OH stretching vibrations (3400–3800 cm^{-1}), only one representative spectrum was resolved, the same that was presented and initially interpreted by Pieczka et al. (2018).

An initial resolution of the recorded spectrum was done in the range of 3400–3800 cm^{-1} applying the FITYK program for data processing and nonlinear curve fitting (Wojdyr 2010), after subtracting a linear background. To identify hidden bands, peak positions, full-widths at half maximum (FWHM), and integrated intensities were determined by fitting with pseudo-Voigt (PV) functions PV = x·Lorentz + (1–x)·Gauss, with x varying in the range from 0 (0 %) to 1 (100 %), applying the Levenberg-Marquardt algorithm (Levenberg 1944; Marquardt 1963). Although good fits with $R^2 > 0.995$ of input models to the empirical spectrum were easily achieved, the theoretical Y- and W-site occupants in these models differ to the occupants as determined by EPMA and SREF, probably due to different fractions of the Lorentzian and Gaussian components in the fitted component bands. Additionally, initial bands with small intensities very often have been eliminated during fitting by their addition to nearby more intense bands by increasing of their Lorentzian component. Therefore, the final fitting was performed on an input model of component bands with Gaussian function shapes and application of the Levenberg-Marquardt fitting method. Spectral position, height and FWHM of each anticipated band was matched in such a way to minimize difference between the empirical spectrum and the theoretical spectrum designated as the sum of intensities of the anticipated bands, considering (1) fine structure of the spectrum and information on spectral positions and assignments of O–H stretching vibrations in Li-bearing tourmalines (Gonzalez-Carreño et al. 1988; Hoang et al. 2011; Skogby et al. 2012; Fantini et al. 2014; Watenphul et al. 2016a; Mercurio et al. 2018; Bronzova et al. 2019), and (2) crystal-chemical data of the studied tourmaline making possible explanation of the component bands by local ^{V}OH and ^{W}OH short-range arrangements. A weak band ~3450 cm^{-1} with a total

intensity ~3.5–3.6 % of the total spectrum (tested with various variants of the spectrum deconvolution) was related to a fluorescence band. The spectrum was slightly smoothed prior the fitting procedure to better isolate the peak maxima, first of all for bands above 3600 cm^{-1} with very small intensities.

RESULTS AND DISCUSSION

Crystal structure

By using the refinement and the chemical data, the Zn-rich fluor-elbaite features the following average empirical formula:

$^{X}(Na_{0.84}\square_{0.14}Ca_{0.01})_{\Sigma 1.00}{}^{Y}(Al_{1.06}Li_{0.84}Zn_{0.69}Fe^{2+}_{0.32}Mn_{0.09})_{\Sigma 3.00}{}^{Z}Al_6(BO_3)_3(^{T}Si_6O_{18})^{V}(OH)_3{}^{W}(F_{0.65}OH_{0.26}O_{0.09})$. Its structure was refined with $R1$ value of 1.67% for 2304 reflections. The refined unit-cell parameters of the tourmaline are: a = 15.921(1), c = 7.127(1) Å and V = 1564.5(3) $Å^3$. In the refinement, the T, B, Z and V sites were fixed with complete occupancies by Si, B, Al and OH, respectively, in accordance with the average distances and with many other Al-rich and Li-bearing tourmalines (e.g. Donnay and Barton 1972; Burns et al. 1994; Shtukenberg et al. 2007; Ertl et al. 2013). Although the T site in Al-rich, Li-bearing tourmalines may sometimes exhibit a small amount of tetrahedrally coordinated boron, the refined <T–O> mean distance of 1.6197(5) Å, is within one standard deviation identical with the <Si–O> bond length for tourmaline as given by MacDonald and Hawthorne (1995) and Bosi and Lucchesi (2007), which were estimated as 1.620 Å and 1.619(1) Å, respectively. This indicates that the T site of this tourmaline is filled exclusively by Si. This is also in agreement (within 1 sd) with the SiO_2 measured by EPMA [6.04(8) apfu, Table 1]. The B site is occupied only with boron, as the refined mean bond length <B–O> = 1.375(1) Å is compatible with a distance 1.374(2) Å evaluated by Bosi and Lucchesi (2007) for tourmalines with the site completely filled with B^{3+}. Similarly, the Z site features a

<Z–O> distance of 1.9087(6) Å, also similar with such distances of other Li-bearing tourmalines where the Z site is completely filled by Al (e.g. Donnay and Barton 1972, Burns et al. 1994; Shtukenberg et al. 2007; Ertl et al. 2013). The refined X-site occupancy [<X–O> = 2.685(1) Å], corresponding to the presence at the site 0.821(6) Na apfu, agrees within 2 sd with the occupancy of the site by 0.85(1) Na + 0.01(0) Ca apfu [9.0(1) refined eps (electrons per a site) vs 9.6(2) eps calculated from the empirical formula]. The refined Y-site occupancy, $Zn_{0.477(1)}Li_{0.523(1)}$, indicating the refined site scattering of 15.87(3) eps corresponds to the estimated site population $(Al_{1.06}Li_{0.84}Zn_{0.69}Fe^{2+}_{0.32}Mn_{0.09})_{\Sigma 3.00}$, and the refined and calculated on the basis of Shannon's (1976) ionic radii <Y–O> mean bond lengths, 2.038(1) Å and 2.040 Å, respectively, are also the same. The occupancy of the V sites was fixed to 3 OH pfu with the refined V[=O(3)]–H(3) distance of 0.819 Å, showing a weak hydrogen bond with oxygen from O(5). The refined W-site occupancy, $F_{0.57(5)}O_{0.43(5)}$, is in good agreement with the microprobe data of F equal to 0.65(4) apfu [8.57(5) eps vs 8.65(4) eps, respectively].

Micro-Raman spectroscopy

Although Raman and IR studies of tourmalines refer usually to the Si_6O_{18} rings, BO_3 groups and OH groups, all previous researchers agree that the O–H stretching vibrations in the range 3000–4000 cm^{-1}, carry the highest portion of crystal chemical and structural information (Gonzalez-Carreño et al. 1988, Hoang et al. 2011; Skogby et al. 2012; Zhao et al. 2012; Fantini et al. 2014; Bosi et al. 2015, 2016; Berryman et al. 2016; Kutzschbach et al. 2016; Watenphul et al. 2016a; Mercurio et al. 2018; Bronzova et al. 2019). This is a result of the specific location of the ^{V}OH and ^{W}OH groups in the tourmaline structure because the ligands are bonded to the octahedrally-coordinated occupants of the Y- and Z-sites, which are the two sites with the highest diversification in cation populations. Therefore, we agree with such statements as, for example, with Watenphul et al. (2016a) that "the stretching modes of the OH groups in the V and W sites

are good candidates for establishing the functional relationship between Raman peak parameters and the crystal chemistry of tourmaline". Furthermore, it should be possible to use this relationship for a fast evaluation of the Y- and W-site populations for other Al-rich and Li-bearing tourmalines, when we are able to decode this relationship. Hence, we must consider that the O–H stretching vibration range reflects quantitatively the chemical bonds of all OH groups from the V and W sites together with all bonded octahedral cations, and additionally, being under the influence of valence-varying X-site occupants (Ca^{2+}, Na^{+} and K^{+}, and a formally zero-valence vacancy) and W-site occupants (OH^{-}/F^{-}, O^{2-}).

As our tourmaline is a fluor-elbaite, its crystal chemistry and structure is expected to be less complex: the Z site can be assumed to be occupied completely by Al, i.e. without a noticeable disordering of Y- and Z-site cations like Mg or Fe, and the V sites can be assumed to be completely occupied by OH, assumptions shown to be valid in many previous studies of Al-rich and Li-bearing tourmalines. The structure refinement results of the studied fluor-elbaite presented above are consistent with this structural model. This restricts our band interpretation to an analysis of local arrangements around the ^{V}OH and ^{W}OH sites in dependence on the Y-site occupancy. Such a model of interpretation of O–H stretching modes in Raman or IR spectra of tourmalines is applied commonly, e.g. Gonzalez-Carreño et al. (1988), Hoang et al. (2011), Skogby et al. (2012), Zhao et al. (2012), Fantini et al. (2014), Bosi et al. (2015), Berryman et al. (2016), Kutzschbach et al. (2016), Mercurio et al. (2018), Bronzova et al. (2019). Applying this model, we will show that Raman spectroscopy of a Al-rich and Li-bearing tourmaline together with a proper deconvolution of its spectrum leads to Y- and W-site occupancies comparable with those derived from single-crystal X-ray diffraction.

Watenphul et al. (2016a) presented an alternative interpretation of the ^{V}OH stretching modes based on the site-symmetry analysis, which led to the assumption that H atoms of the ^{V}OH

groups are related by rotation around the 3-fold axis and collectively participate in a single phonon mode. In consequence, the energy of the ^{V}O–H stretching band should be affected by local cation arrangements associated with all the three ^{V}OH groups bonded to all cations of the octahedral cluster, which schematically may be presented as $^{V}(OH)_3$-[YZZ–YZZ–YZZ]. This model was also used by Bosi et al. (2016) in studies of thermal stability of the octahedral clusters in dravite. In contrast, the model exploring individual local arrangements around each of the three ^{V}OH groups takes into account the influence of 1/3 portion of the octahedral cluster [(^{V}OH–YZ_2]$_3$ developed around the 3-fold axis (the W site is omitted in the two schemes) modifying the energy of the ^{V}O–H stretching band in the single ^{V}OH group. Schematically it may be presented as ^{V}OH-[YZZ]. To explain why we finally decided to employ the short-range arrangement model for the interpretation of our tourmaline spectrum, we first will have to discuss the results of the deconvolution of the Zn-rich fluor-elbaite spectrum, consistent with the assumption of Watenphul et al. (2016a).

Figure 2a presents Raman spectrum of the Zn-rich fluor-elbaite in the range of O–H stretching modes (3400–3800 cm^{-1}). The spectrum has three intense peaks with the maxima at 3497, 3561 and 3597 cm^{-1}. Peaks with similar Raman shifts in the spectrum of elbaite (3494±8, 3562±4 and 3593±4 cm^{-1}) were assigned by Watenphul et al. (2016a) to ^{V}O–H stretching modes related to the octahedral clusters: $^{Y}Li^{Z}Al^{Z}Al$-($^{Y}Al^{Z}Al^{Z}Al)_2$, ($Y^{2+Z}Al^{Z}Al)_2$-$^{Y}Al^{Z}Al^{Z}Al$ and ($^{Y}Li^{Z}Al^{Z}Al)_2$-$^{Y}Al^{Z}Al^{Z}Al$, where Y^{2+} denotes the total of all divalent Y-site occupants (Y^{2+} = $^{Y}Fe^{2+}$ + $^{Y}Mn^{2+}$ + $^{Y}Zn^{2+}$ + $^{Y}Mg^{2+}$). A visible asymmetry of the peak 3497 cm^{-1} centered at ~3475 cm^{-1} would be assigned to the $Y^{2+Z}Al^{Z}Al$-($^{Y}Al^{Z}Al^{Z}Al)_2$ cluster (Watenphul et al. 2016a; Table 3, p.977). The deconvolution of the spectrum in the range of ^{V}O–H stretching modes into four component bands, as was suggested in the paper above, was done with a high R^2 = 99.95 %, with pseudo-Voigt functions and in majority free values of peak center, height and FWHM as presented in the

upper part of Table 2. The fitted component bands 3481.6(9), 3498.9(4), 3560.3(0) and 3596.8(0) cm^{-1} locate within statistical Raman shift ranges as obtained by Watenphul et al. (2016a). However, the contents of ^{Y}Li, Y^{2+} and ^{Y}Al calculated on the basis of the equation given by these authors (see p. 980) for the calculation of specific Y-site occupants on the basis of the band assignments, 0.59 Li, 1.04 Y^{2+} and 1.37 Al apfu, differ significantly from those calculated on the basis of EPMA and SREF: 0.84, 1.10 and 1.06 apfu, respectively. The difference could be a result from the omission of two other possible [YZZ–YZZ–YZZ] clusters. These clusters are connected with ^{V}OH groups that must show up in a Raman spectrum of a Y^{2+}-bearing Li-tourmaline: $^{Y}Li^{Z}Al^{Z}Al$–$Y^{2+Z}Al^{Z}Al$–$^{Y}Al^{Z}Al^{Z}Al$ and $(Y^{2+Z}Al^{Z}Al)_3$. These clusters can be explained due to bond-valence constraints around the W site in the tourmaline structure (Hawthorne 1996, 2002, 2016; Bosi 2013), which allow seven variants of the [YYY] triplet, for which the W site can be occupied by OH^-/F^- or O^{2-} at the simultaneous presence of OH^- at the V site (Table 3). The first of the two arrangements cited above is especially important, because its frequency, compared to the cluster $(Y^{2+Z}Al^{Z}Al)_2$-$^{Y}Al^{Z}Al^{Z}Al$, is commonly higher or at least equal, when the content of Y^{2+} is 2-times higher than the content of Li. Therefore, we also have tested a deconvolution of the spectrum into six ^{V}OH component bands, accepting that the arrangements $(^{V}OH–Y^{2+Z}Al^{Z}Al)_3$, $(^{V}OH–Y^{2+Z}Al^{Z}Al)_2 \times {}^{V}OH–{}^{Y}Al^{Z}Al^{Z}Al$ and $^{V}OH–{}^{Y}Li^{Z}Al^{Z}Al \times {}^{V}OH–Y^{2+Z}Al^{Z}Al \times {}^{V}OH–{}^{Y}Al^{Z}Al^{Z}Al$ could collectively correspond to the band observed at ~3561 cm^{-1}. Results of such a deconvolution that characterizes a similarly high R^2 are presented in Table 2 (lower part) and in Figure 2b. In this case, the integral intensities of the component bands centered at 3477.9(2), 3497.1(1), 3545(1), 3555.7, 3564.2(1) and 3596.3(0) cm^{-1} and their assignments indicate the presence of 0.93 Li, 0.80 Y^{2+} and 1.27 Al apfu, although the contents also differ to the EPMA + SREF results. The discrepancy among the EPMA + SREF contents and the contents estimated on the basis of the equation (directly related to the used interpretation

model) is also visible in Figure 7 in the original paper of Watenphul et al. (2016a), where the deviations among the contents of Y-site occupants, evaluated by applying these two methods, are relatively distinct. In our opinion is this a serious problem of this model, particularly when the Y-site occupants represent a more complicated ternary system (Li^{+}, Y^{2+}, Al^{3+}).

The input model of Raman spectrum in the O–H stretching vibration range

Similarly to other researchers (Gonzalez-Carreño et al. 1988; Hoang et al. 2011; Skogby et al. 2012; Zhao et al. 2012; Fantini et al. 2014; Bosi et al. 2015; Berryman et al. 2016; Kutzschbach et al. 2016; Mercurio et al. 2018; Bronzova et al. 2019) we accept that Raman shifts of the ^{V}O–H stretching bands in tourmaline are dependent on the valence of one bonded Y-site occupant, in Al-rich and Li-bearing tourmalines varying from 3+ to 1+. Because each of the ^{V}OH groups is bonded to one Y and two Z cations and Z site is exclusively occupied by Al as is the case in Al-rich and Li-bearing tourmalines, the only possible arrangements of the [YZZ] triplet around the V site are $^{Y}Al^{Z}Al^{Z}Al$, $Y^{2+Z}Al^{Z}Al$ and $^{Y}Li^{Z}Al^{Z}Al$. The Y cations with different valences shift the electron density away from the ^{V}O–H bond proportionally to its own charge, and as a result, the ^{V}O–H bond length increases, but its strength decreases in accord with the sequence $^{Y}Li^{+}\ldots{}^{V}$O–H through $Y^{2+}\ldots{}^{V}$O–H to $^{Y}Al^{3+}\ldots{}^{V}$O–H. Consequently, ^{Y}Li, Y^{2+} and $^{Y}Al^{3+}$ are assigned to bands with the observed maxima 3597, 3561 and 3497 cm^{-1}, respectively. Because in the tourmaline structure ^{V}OH groups occur with at least 75% abundance relative to the total content of hydroxyls [$3^{V}OH + {}^{W}(OH,F,O)$], the resulting Raman bands have relatively high intensities. An exact observation of the spectrum in Figure 2 allows noticing asymmetry of all the peaks toward lower Raman shifts. Kutzschbach et al. (2016) observed such an effect for the Al-peak in synthetic olenite and interpreted it as a result of the presence of vacancies at the X site. We agree with this interpretation, because an alkali-vacant-type substitution of $X^{+} + Y^{2+} = {}^{X}\square^{0+} + {}^{Y}Al^{3+}$, with Al^{3+} at the Y sites, needs a vacant X site. However, in such a case, we must accept that cations at the

358 remaining two octahedral sites of the [YYY] triplet are also related to this empty X site.
359 Therefore, we should expect for our tourmaline with occupation of the X-site $(Na_{0.84}\square_{0.14}Ca_{0.01})_{\Sigma 1}$
360 the presence of, at least, doubled bands for each absorption peaks previously assigned to the
361 presence of $^{Y}Al^{3+}$, Y^{2+} and ^{Y}Li. In case of a highly diversified X-site population, each of the
362 ^{V}OH-$^{Y}Al^{Z}Al^{Z}Al$ and ^{V}OH-$^{Y}Li^{Z}Al^{Z}Al$ absorption peaks could be deconvoluted even into three
363 bands, related to the presence of vacancy, Na or Ca at the X site, as can be assumed on the basis
364 of the bond-valence constraints around the W site (Hawthorne 1996, 2002, 2016; Bosi 2013) and
365 to the related V-site occupancies (Table 3). All the expectations we considered in an input model
366 of component bands related to the ^{Z}O–H stretching vibrations, assuming the presence of three
367 components for the bands centered at 3497 and 3597 cm^{-1} (influenced by $^{X}\square$, ^{X}Na and ^{X}Ca) and
368 two components for the band centered at 3561 cm^{-1} (influenced only by $\square$ and Na).
369 The ^{W}OH hydroxyls are bonded to three Y cations and influenced by the X-site occupant, e.g.
370 Gonzalez-Carreño et al. (1988), Berryman et al. (2016), Bronzova et al. (2019). The presence of
371 Al, Y^{2+} and Li at the Y site of the studied Zn-rich fluor-elbaite results in ten variants of the
372 [YYY] triplet, from which only seven variants are allowed through bond-valence constraints
373 around the W site (Hawthorne 1996, 2002, 2016; Bosi 2013) as presented in Table 3. It allows to
374 expect that at a small proportion of ^{W}OH in the total OH content ($\leq$ 25 %), the abundances of
375 individual [YYY] arrangements and corresponding intensities of component bands should only
376 be subordinate. Therefore, they only have a potential to modify the basic pattern of the spectrum
377 produced essentially by ^{V}OH bands at lower Raman shift values. Because H^{+} of the ^{W}OH group
378 receives repulsion from the charge of the X cation, the ^{W}O–H length is the longest at a vacant X
379 site, shorter when the X-site is occupied by Na, and the shortest for $^{X}Ca^{2+}$, and is inversely
380 proportional to the respective bond strengths. Therefore, in a tourmaline spectrum ^{W}O–H...$^{X}\square$
381 bands should occur at relatively low Raman shifts ~3600–3650 cm^{-1} (a weak band at ~3615 cm^{-1}

is still assigned by us to ^{V}OH groups bonded to $^{Y}Li^{+Z}Al^{Z}Al\ldots{}^{X}Ca$), ^{W}O–H...^{X}Na around 3700 cm^{-1} (Hoang et al. 2011; Skogby et al. 2012; Fantini et al. 2014; Berryman et al. 2016; Watenphul et al. 2016a), and ^{W}OH-$^{Y}Al^{Y}Li^{Y}$Li...^{X}Ca and ^{W}OH-$Y^{2+}Y^{2+Y}$Li...^{X}Ca bands might be expected above to 3700–3750 cm^{-1}. Applying to the [YYY] arrangements the same reasoning as those used above for the [YZZ] triplets, it can be expected that the strongest effect of shifting the electron density away from the ^{W}O–H bond would take place for a $^{Y}AlY^{2+}Y^{2+}$ arrangement, and the weakest for the $^{Y}Al^{Y}Li^{Y}$Li triplet. Consequently, the ^{W}O–H bond should be the weakest in case of the first-type triplet, and the strongest for the last. Summarizing, considering bond-valence constraints around the W site (Hawthorne 1996, 2002, 2016; Bosi 2013), the combination of ^{W}OH...X and ^{W}OH...[YYY] effects should result in a spectrum as maximum nine component bands (Table 3) with low intensities, totally ≤25 % of the whole spectrum, occurring in the spectral range of ~3600 to ~3800 cm^{-1}. In consequence, our input model for a deconvolution of the spectrum of Zn-bearing and Ca-poor fluor-elbaite comprises eight component bands, related to ^{V}O–H stretching modes and nine component bands related to ^{W}O–H stretching modes, both modified by the Y-site occupants and influenced by ^{X}□, ^{X}Na or ^{X} Ca.

Fitting of the input model

Figure 3 and Table 4 present fitting results of the O–H stretching vibration range in the Zn-bearing fluor-elbaite. The three asymmetrical peaks related to ^{V}O–H modes, centered at 3497, 3561 and 3597 cm^{-1}, were resolved into 3 + 2 + 3 component bands, respectively. We interpret them as $^{Y}Al^{Z}Al^{Z}$Al, $Y^{2+Z}Al^{Z}$Al and $^{Y}Li^{Z}Al^{Z}$Al arrangements modified by the presence of □ (the component band with the lowest Raman shift in each peak), Na^{+} or Ca^{2+} at the X site (the component band with the highest Raman shift in the first and third peak). Total intensities of the component bands corresponding to the presence of ^{Y}Al, Y^{2+} or ^{Y}Li at the triplets ^{V}OH-[YZZ], i.e.

405 $^{V}OH I_{^{Y}Al^{Z}Al^{Z}Al}$, $^{V}OH I_{Y^{2+Z}Al^{Z}Al}$ and , $^{V}OH I_{^{Y}Li^{Z}Al^{Z}Al}$, in relation to their sum, $^{V}OH I_{Y^{Z}Al^{Z}Al}$, give
406 shares of the Y constituents (Al, Y^{2+} and Li) in the Y-site occupancy: ~37.4, 37.4 and 25.2 %,
407 respectively, which corresponds to the [YYY] triplet $(Al_{1.12}Y^{2+}_{1.12}Li_{0.76})_{\Sigma 3}$. Furthermore, the ratio
408 of total intensity of the ^{V}OH bands, $^{V}OH I_{Y^{Z}Al^{Z}Al}$, in relation to the total intensity of the ^{V}OH and
409 ^{W}OH bands, $^{V}OH I_{Y^{Z}Al^{Z}Al} + {}^{W}OH I_{YYY}$, allows estimating an approximate $^{W}OH_{Raman}$ content from
410 the equation: $^{W}OH = [3 \times (^{V}OH I_{Y^{Z}Al^{Z}Al} + {}^{W}OH I_{YYY}) / {}^{V}OH I_{Y^{Z}Al^{Z}Al} - 3]$ (apfu). For the studied
411 fluor-elbaite the ^{W}OH content evaluated in such a way is ~0.16 apfu. The contents of 1.12 ^{Y}Al,
412 1.12 Y^{2+}, 0.76 ^{Y}Li apfu and 0.16 ^{W}OH groups pfu, estimated directly from the Raman spectrum
413 of the fluor-elbaite after the deconvolution of the O–H stretching vibration range, correspond
414 well to the EPMA + SREF results: 1.06 Al, 1.10 Y^{2+}, 0.84 Li and 0.26 OH apfu. As a result, the
415 output model of component bands in the OH stretching vibration range of the fluor-elbaite
416 ascribes its empirical spectrum with a R^2 value of 0.9998, better than in the case of the previously
417 discussed model of Watenphul et al. (2016a).
418 A deconvolution of the spectrum gives also an opportunity to use one of a few parameters,
419 which are possible to evaluate on basis of its quantitative results in the calculation of the crystal
420 chemical formula, similarly as it was done e.g. for Li. Lithium can not be analyzed by
421 conventional microprobe, but evaluated on the basis of the EPMA results and the Y-site
422 scattering from SREF. The introduction of such a parameter into the procedure of the formula
423 calculation gives the opportunity to evaluate ^{Y}Li and ^{W}OH by matching of such Li_2O and H_2O
424 amounts (in wt %) to obtain the value of the parameter matched to the value evaluated from the
425 spectrum deconvolution. As the most suitable parameter we determined the content of the ^{V}OH-
426 $^{Y}Al^{Z}Al^{Z}Al$ component bands in the total spectrum, i.e. the ratio $^{V}OH I_{^{Y}Al^{Z}Al^{Z}Al} / (^{V}OH I_{YZZ} +$

$^{W}OH_{I_{YYY}}$). This is due to the only small superposition of the ^{V}OH-$^{Y}Al^{Z}Al^{Z}Al$ component bands, influenced by ^{X}(□, Na, Ca) with the remaining part of the spectrum, which gives the opportunity to evaluate the parameter with a relatively high accuracy. The crystal chemical formula calculated in such a way (only on basis of the EPMA and RS results) for the studied fluor-elbaite (Table 1) is as follows: $^{X}(Na_{0.85}\square_{0.14}Ca_{0.01})_{\Sigma 1.00}{}^{Y}(Al_{1.11}Y^{2+}{}_{1.11}Li_{0.78})_{\Sigma 3.00}{}^{Z}Al_6(BO_3)_3(Si_6O_{18})(OH)_3(F_{0.65}OH_{0.13}O_{0.22})$. It differs from the EPMA + SREF formula by +0.05 Al, +0.01 Y^{2+} and -0.06 Li apfu.

IMPLICATIONS

The empirical EPMA and SREF formula of the studied Zn-rich fluor-elbaite is $^{X}(Na_{0.85}\square_{0.14}Ca_{0.01})_{\Sigma 1.00}{}^{Y}(Al_{1.06}Li_{0.84}Zn_{0.69}Fe^{2+}{}_{0.32}Mn_{0.09})_{\Sigma 3.00}{}^{Z}Al_6(BO_3)_3(Si_6O_{18})(OH)_3(F_{0.65}OH_{0.26}O_{0.09})$. Our interpretation of the RS of the tourmaline in the range of O–H stretching modes, 3400–3800 cm^{-1}, indicates the presence of 1.12 Al, 1.12 Y^{2+} and 0.76 Li apfu in the [YYY] triplet bonded to three ^{V}OH groups, and with OH, F and O, which occupy the W site. The ^{W}OH content deduced on the basis of the deconvolution of the spectrum is ~0.16 apfu, which leads to the W-site occupation $(F_{0.65}O_{0.19}OH_{0.16})_{\Sigma 1}$. An application of the ratio $^{V}OH_{I_{Y}Al^{Z}Al^{Z}Al}$ / ($^{V}OH_{I_{YZZ}}$ + $^{W}OH_{I_{YYY}}$), which reflects the contribution of ^{V}OH groups bonded to ^{Y}Al in relation to the total content of ^{V+W}OH groups, as an additional criterion in the formula calculation allows to re-calculate it as $^{X}(Na_{0.85}\square_{0.14}Ca_{0.01})_{\Sigma 1.00}{}^{Y}(Al_{1.11}Y^{2+}{}_{1.11}Li_{0.78})_{\Sigma 3.00}{}^{Z}Al_6(BO_3)_3(Si_6O_{18})(OH)_3(F_{0.65}OH_{0.13}O_{0.22})$, where Y^{2+} = Zn + Fe + Mn, based only on EPMA and RS results. The <Y–O> mean bond length calculated on the basis of the formula, 2.036 Å, as well as electron densities at the X, Y and W sites, 9.6, 16.1 and 8.7 eps respectively, agree well with the refined values (within ~2 sd SREF

and EPMA results). Taken into account that in the applied methods (SREF, RS) the crystal chemical and structural information was collected from volumes of the investigated crystal having different dimensions, i.e. ~1 μm^3 in RS vs several μm^3 in EPMA compared to a significantly larger volume of ~3×10^6 μm^3 for the single-crystal X-ray diffraction, the accordance of both formulae in the order of +0.05 Al, +0.01 Y^{2+} and -0.06 Li apfu, i.e. within 1 sd of the microprobe Al and Y^{2+} determinations is an excellent agreement. Compared to the results of the deconvolution and interpretation of the spectrum, as was suggested by Watenphul et al. (2016a), +0.31 Al, -0.06 Y^{2+}, -0.25 Li apfu (deconvolution of the spectrum into 4 ^{Z}OH component bands), or + 0.21 Al, -0.30 Y^{2+}, +0.09 Li apfu, (deconvolution into 6 ^{Z}OH component bands), our new proposed method gives results in better agreement with the EPMA and SREF results. Considering the standard deviations of the refined parameters (including site scattering) of the structure refinement, our (EPMA + RS)-evaluated formula actually seems to be very close to the calculated Y-site occupants (based on the EPMA + SREF results). Assuming Y-site scattering errors in the range of +1 to +3 sd, the differences between the (EPMA + RS)-evaluated Y-site contents (Al, Y^{2+}, Li) and those calculated from EPMA + SREF differ only by ±0.01 apfu per 1 sd at maximum (Table 1).

The presented results are the first documented case with the application of RS for the evaluation of the chemistry of a Li-bearing tourmaline. Up until now, only Watenphul et al. (2016b) attempted to apply RS to the discrimination of tourmaline species, which they showed was useful for discrimination of Mg- and Fe-dominant tourmaline species. Our presented method needs subsequent investigations for Al-rich and Li-bearing tourmalines representing other mineral species (elbaite, fluor-elbaite, fluor-liddicoatite, rossmanite, darrellhenryite), which additionally could validate it and should allow to obtain the influence of the orientation to the

crystal faces and the precision of the Li and OH evaluation and ^{W}OH band assignments. More researches about that are in progress. However, it seems that RS can be a very important tool in the achievement of crystal chemical and structural information from ultra-small portions of a crystal, even smaller than needed for a single-crystal X-ray diffraction. Generally, it should not be surprising, because it is obvious that single-crystal X-ray diffraction and Raman spectroscopy present two different patterns of the same crystal structure and code the same crystal chemical and structural information, but in a different way. A crystal structure refinement uses the intensities and positions of X-ray diffraction reflections, while Raman spectroscopy uses intensities and positions of absorption bands.

The determination of Li (Li_2O) in Li-tourmalines is still problematic. Rinaldi and Llovet (2015) stated that a new WDS soft X-ray emission spectrometer (SXES) introduced by one of the two main EPMA equipment manufactures opens a whole new perspective for the analysis of light elements (including Li) and low-energy lines of other elements in the nearest future. However, because Li can still not be analyzed by conventional EPMA instruments, for large and homogeneous crystals this difficulty can only be omitted by a direct analysis of Li, e.g. with AAS or LA-ICP-MS. These methods cannot be used for very small crystals, which show a complex zonation within a distance of a few μm. Tempesta and Agrosì (2016) studied the chemistry of red beryls (including Li) with approximately 10 μm spot sizes by using Laser Induced Breakdown Spectroscopy (LIBS), however, although this method is fast and only minimally destructive, it works without standards but yields quantitative results very close to those obtained with conventional techniques. Although the Li amount can be approximately evaluated on basis of single-crystal X-ray diffraction, this method, currently mainly available at faculties of chemistry, is not always accessible for mineralogists and cannot be applied routinely. To solve this problem,

Pesquera et al. (2016) derived a statistical equation allowing the calculation of Li_2O content in wt% from the amounts of main oxide components of Li-bearing tourmalines such as SiO_2, Al_2O_3, total Fe as FeO and MnO. However, as shown by Pieczka et al. (2018), this method does not work well, if a tourmaline is enriched by an atypical component, e.g. ZnO and even CaO, which are often present as important constituents in Al-rich, Li-bearing tourmalines. In this light, our presented method, providing comparable Li contents, estimated by the solution of O–H stretching vibration modes of a Raman spectrum of Li-tourmaline, can be applied relatively easily and quickly compared to single-crystal X-ray diffraction refinements. All the previous remarks refer also to the quantitative evaluation of OH_{total} (H_2O), another important component, which is usually not analyzed and only calculated on basis of an assumed tourmaline stoichiometry. Raman spectroscopy gives an opportunity to determine the relatively exact amount of OH, although the V sites must be assumed the be fully occupied by OH. Hence, the amount of ^{W}OH can be determined as an excess above 3 anions pfu. We consider that by the chemical analysis with EPMA-WDS and by using Raman spectroscopy it is possible to receive the correct crystal chemical and structural formula of a Al-rich and Li-bearing tourmaline in a relatively short time without the necessity of comprehensive structural studies by single-crystal X-ray diffraction.

ACKNOWLEDGEMENTS AND FOUNDING

We thank two anonymous reviewers and the technical reviewer for their comments that were very helpful to improve the manuscript. We are also very indebted to Edward S. Grew for the careful editorial handling. This study was supported by the National Science Centre (Poland) grant 2015/19/B/ST10/01809 and AGH UST grant 16.16.140.315, both to AP, and in part by the Austrian Science Fund (FWF) project no. P 31049-N29 (AE).

519

520 **REFERENCES CITED**

521 Baksheev, I.A. and Kudryavtseva, O.E. (2004) Nickeloan tourmaline from the Berezovskoe gold
522 deposit, Middle Urals, Russia. Canadian Mineralogist, 42, 1065–1078.
523 Berryman, E.J., Wunder, B., Ertl, A., Koch-Müller, M., Rhede, D., Scheidl, K., Giester, G. and
524 Heinrich, W. (2016) Influence of the X-site compositionon tourmaline's crystal structure:
525 Investigation of synthetic K-dravite, dravite, oxy-uvite, and magnesio-foitite using SREF and
526 Raman spectroscopy. Physics and Chemistry of Minerals, 43, 83–102.
527 Bosi, F. (2013) Bond-valence constraints around the O1 site of tourmaline. Mineralogical
528 Magazine, 77, 343–351.
529 Bosi, F. and Lucchesi, S. (2007) Crystal chemical relationships in the tourmaline group:
530 structural constraints on chemical variability. American Mineralogist, 92, 1054–1063.
531 Bosi, F., Skogby, H., Lazor, P. and Reznitskii, L. (2015) Atomic arrangements around the O3 site
532 in Al- and Cr-rich oxy-tourmalines: a combined EMP, SREF, FTIR and Raman study. Physics
533 and Chemistry of Minerals, 42, 441–453.
534 Bosi, F., Skogby, H. and Balić-Žunić, T. (2016) Thermal stability of extended clusters in dravite:
535 a combined EMP, SREF and FTIR study. Physics and Chemistry of Minerals, 43, 395–407.
536 Bosi, F., Cámara, F., Ciriotti, M.E., Hålenius, U., Reznitskii, L. and Stagno, V. (2017) Crystal-
537 chemical relations and classification problems of tourmalines belonging to the oxy-schorl–
538 oxy-dravite–bosiite–povondraite series. European Journal of Mineralogy, 29, 445–455.
539 Bronzova, Y., Babushkina, M., Frank-Kamenetskaya, O., Vereshchagin, O., Rozhdestvenskaya,
540 I. and Zolotarev, A. (2019) Short-range order in Li-Al tourmalines: IR spectroscopy, X-ray
541 single crystal diffraction analysis and bond valence theory approach. Physics and Chemistry of
542 Minerals, 46, 815–825.

543 Burns, P.C., MacDonald, D.J., and Hawthorne, F.C. (1994) The crystal chemistry of manganese-
544 bearing elbaite. Canadian Mineralogist, 32, 31–41.
545 Donnay, G. and Barton, R. Jr. (1972) Refinement of the crystal structure of elbaite and the
546 mechanism of tourmaline solid solution. TMPM Tschermaks Mineralogische und
547 Petrographische Mitteilungen, 18, 273–286.
548 Ertl, A., Marschall, H.R., Giester, G., Henry, D.J., Schertl, H.-P., Ntaflos, T., Luvizotto, G.L.,
549 Nasdala, L. and Tillmanns, E. (2010) Metamorphic ultra high-pressure tourmalines: Structure,
550 chemistry, and correlations to PT conditions. American Mineralogist, 95, 1–10.
551 Ertl, A., Giester, G., Schüssler, U., Brätz, H., Okrusch, M., Tillmanns, E. and Bank, H. (2013)
552 Cu- and Mn-bearing tourmalines from Brazil and Mozambique: crystal structures, chemistry
553 and correlations. Mineralogy and Petrology, 107, 265–279.
554 Fantini, C., Tavares, M.C., Krambrock, K., Moreira, R.L. and Righi, A. (2014) Raman and
555 infrared study of hydroxyl sites in natural uvite, fluor-uvite, magnesio-foitite, dravite and
556 elbaite tourmalines. Physics and Chemistry of Minerals, 41, 247–254.
557 Ferreira, A.C.M., Ferreira, V.P., Soares, D.R. and Vilarroel-Leo, H.S. (2005) Chemical and
558 mineralogical characterization of elbaite from the Alto Quixaba pegmatite, Seridó Province,
559 NE Brazil. Anais da Academia Brasileira de Ciências, 77, 729–743.
560 Gonzalez-Carreño, T., Fernandez, M. and Sanz, J. (1988) Infrared and electron microprobe
561 analysis of tourmalines. Physics and Chemistry of Minerals, 15, 452–460.
562 Hawthorne, F.C. (1996) Structural mechanisms for light-element variations in tourmaline.
563 Canadian Mineralogist, 34, 123–132.
564 Hawthorne, F.C. (2002) Bond-valence constraints on the chemical composition of tourmaline.
565 Canadian Mineralogist, 40, 789–797.

566 Hawthorne, F.C. (2016) Short-range atomic arrangements in minerals. I: The minerals of the
567 amphibole, tourmaline and pyroxene supergroups. European Journal of Mineralogy, 28, 513–
568 536.
569 Henry, D.J. and Dutrow, B.L. (1996) Metamorphic tourmaline and its petrologic applications.
570 Reviews in Mineralogy and Geochemistry, 33, 503–557.
571 Henry, D.J., Novák, M., Hawthorne, F.C., Ertl, A., Dutrow, B.L., Uher, P. and Pezzotta, F.
572 (2011) Nomenclature of the tourmaline-supergroup minerals. American Mineralogist, 96,
573 895–913.
574 Hoang, L.H., Hien, N.T.M.; Chen, X.B., Minh, N.V. and Yang, I.-S. (2011) Raman spectroscopic
575 study of various types of tourmalines. Journal of Raman Spectroscopy, 42, 1443–1446.
576 Kutzschbach, M., Wunder, B., Rhede, D., Koch-Müller, M., Ertl, A., Giester, G., Heinrich, W.
577 and Franz, G. (2016) Tetrahedral boron in natural and synthetic HP/UPH tourmaline:
578 Evidence from Raman spectroscopy, EMPA, and sinfle-crystal XRD. American Mineralogist,
579 101, 93–104.
580 Levenberg, K. (1944) A method for the solution of certain non-linear problems in least squares.
581 Quarterly of Applied Mathematics, 2, 164–168.
582 Lottermoser, B.G. and Plimer, I.R. (1987) Chemical variation in tourmalines, Umberatana, South
583 Australia. Neues Jahrbuch für Mineralogie Monatshefte, 1987, 7, 314–326.
584 Lussier, A., Ball, N.A., Hawthorne, F.C., Henry, D.J., Shimizu, R., Ogasawara, Y. and Ota, T.
585 (2016) Maruyamaite, $K(MgAl_2)(Al_5Mg)Si_6O_{18}(BO_3)_3(OH)_3O$, a potassium-dominant
586 tourmaline from the ultrahigh-pressure Kokchetav massif, northern Kazakhstan: Description
587 and crystal structure. American Mineralogist, 101, 355–361.
588 MacDonald, D.J. and Hawthorne, F.C. (1995) The crystal chemistry of Si ↔Al substitution in
589 tourmaline. Canadian Mineralogist, 33, 849–858.

590 Marquardt, D. (1963) An algorithm for least-squares estimation of nonlinear parameters". SIAM
591 Journal on Applied Mathematics, 11, 431–441.
592 Mercurio, M., Rossi, M., Izzo, F., Cappelletti, P., Germinario, C., Grifa, C., Petrelli, M., Vergara,
593 A. and Langella, A. (2018) The characterization of natural gemstones using non-invasive FT-
594 IR spectroscopy: New data on tourmalines. Talanta, 178, 147–159.
595 Pesquera, A., Gil-Crespo, P.P., Torres-Ruiz, F., Torres-Ruiz, J. and Roda-Robles, E. (2016) A
596 multiple regression method for estimating Li in tourmaline from electron microprobe analyses.
597 Mineralogical Magazine, 80, 1129–1133.
598 Pieczka, A., Gołębiowska, B., Jeleń, P., Włodek, A., Szełęg, E. and Szuszkiewicz, A. (2018)
599 Towards Zn-dominant tourmaline: a case of Zn-rich fluor-elbaite and elbaite from the Julianna
600 system at Piława Górna, Lower Silesia, SW Poland. Minerals, 8, 126.
601 Pouchou, J.-L. and Pichoir, F. (1991) Quantitative analysis of homogeneous or stratified
602 microvolumes applying the model "PAP". In Electron Probe Quantitation; Heinrich, K.F.J.,
603 Newbury, D.E., eds., Plenum Press: New York, NY, USA, 1991; pp. 3l–75.
604 Rinaldi, R. and Llovet, X. (2015) Electron Probe Microanalysis: A Review of the Past, Present,
605 and Future. Microscopy and Microanalysis, 21, 1053–1069.
606 Shannon, R.D. (1976) Revised effective ionic radii and systematic studies of interatomic
607 distances in halides and chalcogenides. Acta Crystallographica, A32, 751–767.
608 Sheldrick, G.M. (1998) SHELXL97, Release 97-2. Program for crystal structure refinement.
609 University of Göttingen, Göttingen, Germany.
610 Shtukenberg, A., Rozhdestvenskaya, I., Frank-Kamenetskaya, O., Bronzova, J., Euler, H., Kirfel,
611 A., Bannova, I. and Zolotarev, A. (2007) Symmetry and crystal structure of biaxial elbaite-
612 liddicoatite tourmaline from the Transbaikalia region, Russia. American Mineralogist, 92,
613 675–686.

614 Skogby, H., Bosi, F. and Lazor, P. (2012) Short-range order in tourmaline: a vibrational
615 spectroscopic approach to elbaite. Physics and Chemistry of Minerals, 39, 811–816.
616 Sokolov, M. and Martin, R.F. (2009) A Pb-dominant member of the tourmaline group, Minh Tien
617 granitic pegmatite, Luc Yen District, Vietnam. Estudos Geológicos, 19, 352–353.
618 Sokolov, P.B., Gorskaya, M.G. and Kretser, Yu.L. (1988) Zinc-bearing tourmalines from rare-
619 metal pegmatites. Zapiski Vsesoyuznogo Mineralogicheskogo Obshchestva, 117, 70–74. (in
620 Russian).
621 Szuszkiewicz, A., Szełęg, E., Pieczka, A., Ilnicki, S., Nejbert, K., Turniak, K., Banach, M.,
622 Łodziński, M., Różniak, R. and Michałowski, P. (2013) The Julianna pegmatite vein system at
623 the Piława Górna mine, Góry Sowie Block, SW Poland - preliminary data on geology and
624 descriptive mineralogy. Geological Quarterly, 57, 467–484.
625 Tempesta, G. and Agrosì, G. (2016) Standardless, minimally destructive chemical analysis of red
626 beryls by means of Laser Induced Breakdown Spectroscopy. European Journal of Mineralogy,
627 28, 571–580.
628 Van Hinsberg, V.J., Henry, D.J. and Dutrow, B.L. (2011) Tourmaline as a petrologic forensic
629 mineral: a unique recorder of its geologic past. Elements, 7, 327–332.
630 Vereshchagin, O.S., Rozhdestvenskaya, I.V., Frank-Kamenetskaya, O.V., Zolotarev, A.A. and
631 Mashkovtsev, R.I. (2013) Crystal chemistry of Cu-bearing tourmalines. American
632 Mineralogist, 98, 1610–1616.
633 Vezzoni, S., Biagioni, C., D'Orazio, M., Pieruccioni, D., Galanti, Y., Petrelli, M. and Molli, G.
634 (2018) Evidence of Permian magmatism in the Alpi Apuane metamorphic complex (Northern
635 Apennines, Italy): New hints for the geological evolution of the basement of the Adria plate.
636 Lithos, 318-319, 104–123.

637 Watenphul, A., Burgdorf, M., Schlüter, J., Horn, I., Malcherek, T. and Mihailova, B. (2016a)
638 Exploring the potential of Raman spectroscopy for crystallochemical analyses of complex
639 hydrous silicates: II. Tourmalines. American Mineralogist, 101, 970–985.
640 Watenphul, A., Schlüter, J., Bosi, F., Skogby, H., Malcherek, T. and Mihailova, B. (2016b)
641 Influence of the octahedral cationic-site occupancies on the framework vibrations of Li-free
642 tourmalines, with implications for estimating temperature and oxygen fugacity in host rocks.
643 American Mineralogist, 101, 2554–2563.
644 Wojdyr, M. (2010) Fityk, a general-purpose peak fitting program. Journal of Applied
645 Crystallography 43, 1126–1128.
646 Zhao, C., Liao, L., Xia, Z. and Sun, X. (2012) Temperature-dependent Raman and infrared
647 spectroscopy study on iron-magnesium tourmalines with different Fe content. Vibrational
648 Spectroscopy, 62, 28–34.
649 Žáček, V., Frýda, J., Petrov, A. and Hyršl, J. (2000) Tourmalines of the povondraite –
650 (oxy)dravite series from the cap rock of meta-evaporite in Alto Chapare, Cochabamba,
651 Bolivia. Journal of the Czech Geological Society, 45, 3–12.
652

This is a preprint, the final version is subject to change, of the American Mineralogist (MSA)
Cite as Authors (Year) Title. American Mineralogist, in press.
DOI: https://doi.org/10.2138/am-2020-7360

Figure captions:

Figure. 1. Back-scattered-electron image (colors added) of zinc-rich fluor-elbaite and schorl from Piława Górna, Lower Silesia, southwestern Poland (enlargement of a part of Pieczka et al. 2018, Fig. 4d). The area analyzed with the electron microprobe, single-crystal X-ray diffraction and Raman spectroscopy is enclosed by a red ellipse.

Figure 2. Deconvolution of the O–H vibration modes in Zn-rich fluor-elbaite with the model of Watenphul et al. (2016a): (a) four ^{V}OH component bands, (b) six ^{V}OH component bands (explanation in the text). Colors in the spectrum: grey – the measured spectrum, black – the smoothed spectrum, red – the fitted model, orange – a fluorescence band, blue – bands of ^{V}O–H vibrations, green – bands of ^{W}O–H vibrations.

Figure. 3. Deconvolution of the O–H vibration modes in Zn-rich fluor-elbaite with the short-range arrangement model. Colors as in Fig. 2.

This is a preprint, the final version is subject to change, of the American Mineralogist (MSA)
Cite as Authors (Year) Title. American Mineralogist, in press.
DOI: https://doi.org/10.2138/am-2020-7360

Table 1. Chemical composition of Zn-rich fluor-elbaite from Piława Górna.

Component	9/1	18/8	20/9	8/4	average (wt%)		average (apfu)	+1sd (apfu)	+2sd (apfu)	+3sd (apfu)	RS (apfu)
SiO_2	36.96	36.10	36.06	37.08	36.55(47)	Si^{4+}	6.04(8)	6.04(8)	6.05(8)	6.05(8)	6.08(8)
Al_2O_3	36.64	35.70	35.75	36.98	36.27(56)	Al^{3+}	7.06(11)	7.06(11)	7.07(11)	7.08(11)	7.11(11)
FeO	2.45	2.37	2.42	1.92	2.29(22)	Fe^{2+}	0.32(3)	0.32(3)	0.32(3)	0.32(3)	0.32(3)
MnO	0.67	0.58	0.61	0.76	0.66(07)	Mn^{2+}	0.09(1)	0.09(1)	0.09(1)	0.09(1)	0.09(1)
ZnO	5.64	5.90	5.57	5.68	5.70(12)	Zn^{2+}	0.69(1)	0.70(1)	0.70(1)	0.70(1)	0.70(2)
CaO	0.07	0.09	0.08	0.10	0.08(01)	Ca^{2+}	0.01(0)	0.01(0)	0.01(0)	0.01(0)	0.01(0)
Na_2O	2.70	2.62	2.61	2.62	2.64(04)	Na^{+}	0.84(1)	0.85(1)	0.85(1)	0.85(1)	0.85(1)
F	1.35	1.18	1.24	1.19	1.24(07)	F^{-}	0.65(4)	0.65(4)	0.65(4)	0.65(4)	0.65(4)
$B_2O_{3(calc.)}$					10.53	B^{3+}	3.00	3.00	3.00	3.00	3.00
$Li_2O_{(calc.)}$					1.26	Li^{+}	0.84	0.83	0.82	0.81	0.78
$H_2O_{(calc.)}$					2.96	OH^{-}	3.26	3.24	3.23	3.21	3.13
$-O=F_2$					-0.52	O^{2-}	27.09	27.11	27.12	27.14	27.22
Total					99.65						

Notes: average analysis – EPMA analysis completed with Li_2O and H_2O amounts matched to the SREF measured Y-site scattering; +1sd, +2sd and +3sd analyses – EPMA analysis completed with Li_2O and H_2O amounts matched to the SREF measured Y-site scattering +1sd, +2sd or +3sd, respectively; RS – EPMA analysis completed with Li_2O and H_2O amounts matched to the $^{V}OH_{I}{}_{Y}Al^{z}Al^{z}Al$ / ($^{V}OH_{I}{}_{YZZ}$ + $^{W}OH_{I}{}_{YYY}$) parameter equal to 0.3558, designed from the deconvoluted Raman spectrum. For the +1sd, +2sd, +3sd and RS analyses contents (in wt%) of the calculated components B_2O_3, Li_2O and H_2O are equal to: 10.52, 10.50, 10.49 and 10.44 (B_2O_3); 1.25, 1.24, 1.22 and 1.16 (Li_2O); 2.94, 2.92, 2.90 and 2.82 (H_2O); totals 99.61, 99.56, 99.52, 99.32, respectively.

This is a preprint, the final version is subject to change, of the American Mineralogist (MSA)
Cite as Authors (Year) Title. American Mineralogist, in press.
DOI: https://doi.org/10.2138/am-2020-7360

Table 2. Deconvolution of O–H stretching bands in Zn-rich fluor-elbaite consistently with the model of Watenphul et al. (2016a)[1]

Raman shift (cm^{-1})	FWHM (cm^{-1})	Integral intensity (%)	Interpretation
3481.6(9)	30.0(6)	15.66	$^{V}OH–Y^{2+Z}Al^{Z}Al \times {}^{V}OH–(^{Y}Al^{Z}Al^{Z}Al)_2$
3498.9(4)	25.7(3)	20.17	$^{V}OH–^{Y}Li^{Z}Al^{Z}Al \times {}^{V}OH–(^{Y}Al^{Z}Al^{Z}Al)_2$
3560.3(0)	28.4(1)	43.11	$(^{V}OH–Y^{2+Z}Al^{Z}Al)_2 \times {}^{V}OH–^{Y}Al^{Z}Al^{Z}Al$
3596.8(0)	21.0(1)	18.65	$(^{V}OH–^{Y}Li^{Z}Al^{Z}Al)_2 \times {}^{V}OH–^{Y}Al^{Z}Al^{Z}Al$
3629.3(3)	8	0.28	$^{W}OH–Y^{2+Y}Al^{Y}Al$ …□
3642.0(8)	8	0.07	$^{W}OH–Y^{2+}Y^{2+Y}Al$ …□
3672.0(3)	10.0(8)	0.40	^{W}OH–YYY…(□,Na)
3682.2(4)	10(1)	0.54	^{W}OH–YYY…Na
3713(1)	39(4)	1.12	^{W}OH–YYY…(Na,Ca)
3477.9(2)	26	11.65	$^{V}OH–Y^{2+Z}Al^{Z}Al \times (^{V}OH–^{Y}Al^{Z}Al^{Z}Al)_2$
3497.1(1)	28.0(2)	26.94	$^{V}OH–^{Y}Li^{Z}Al^{Z}Al \times (^{V}OH–^{Y}Al^{Z}Al^{Z}Al)_2$
3545(1)	24(2)	3.46	$(^{V}OH–Y^{2+Z}Al^{Z}Al)_3$
3555.7	22	12.55	$(^{V}OH–Y^{2+Z}Al^{Z}Al)_2 \times {}^{V}OH–^{Y}Al^{Z}Al^{Z}Al$
3564.2(1)	22	21.65	$^{V}OH–^{Y}Li^{Z}Al^{Z}Al \times {}^{V}OH–Y^{2+Z}Al^{Z}Al \times {}^{V}OH–^{Y}Al^{Z}Al^{Z}Al$
3596.3(0)	22.2(1)	21.05	$(^{V}OH–^{Y}Li^{Z}Al^{Z}Al)_2 \times {}^{V}OH–^{Y}Al^{Z}Al^{Z}Al$
3629.4(5)	8	0.27	$^{W}OH–Y^{2+Y}Al^{Y}Al$ …□
3641.8(4)	8	0.16	$^{W}OH–Y^{2+}Y^{2+Y}Al$ …□
3670.8(4)	9(1)	0.33	^{W}OH–YYY…(□,Na)
3680(1)	16(2)	0.75	^{W}OH–YYY…Na
3713.1(7)	37	1.18	^{W}OH–YYY…(Na,Ca)

[1] – upper part presents the deconvolution into four component bands for ^{V}OH, lower part presents the deconvolution of the spectrum with two additional components (see explanation in the text); FWHM - full widths at half maximum. Data in parentheses are standard deviations. The lack of such data at peak positions or FWHMs denotes that the parameters were fixed.

This is a preprint, the final version is subject to change, of the American Mineralogist (MSA)
Cite as Authors (Year) Title. American Mineralogist, in press.
DOI: https://doi.org/10.2138/am-2020-7360

Table 3. Possible W-[YYY] short-range arrangements in tourmaline with ^{Z}Al and ^{V}OH.

[YYY]	W		
arrangement	X = □	X = Na	X = Ca
[AlAlY^{2+}]	O		
[AlAlLi]	OH/F	OH/F* or O	
[Al$Y^{2+}Y^{2+}$]	OH/F	OH/F	
[AlY^{2+}Li]		OH/F	
[$Y^{2+}Y^{2+}Y^{2+}$]		OH/F	
[AlLiLi]		OH/F*	OH/F
[$Y^{2+}Y^{2+}$Li]			OH/F**

* in elbaite and fluor-elbaite, ** in Y^{2+}-bearing fluor-liddicoatite.

This is a preprint, the final version is subject to change, of the American Mineralogist (MSA)
Cite as Authors (Year) Title. American Mineralogist, in press.
DOI: https://doi.org/10.2138/am-2020-7360

Table 4. Deconvolution of O–H stretching vibration bands in Zn-rich fluor-elbaite according to the short-range arrangement model.

Raman shift (cm^{-1})	FWHM (cm^{-1})	Integral intensity (%)	Interpretation
3450	54		fluorescence
3478.1(3)	28.5	10.14	$^{V}OH–^{Y}Al^{Z}Al^{Z}Al…^{X}\square$
3498.1(1)	28.8(2)	24.96	$^{V}OH–^{Y}Al^{Z}Al^{Z}Al…^{X}Na$
3523.0(3)	10.8(8)	0.48	$^{V}OH–^{Y}Al^{Z}Al^{Z}Al…^{X}Ca$
3538.1(3)	26	5.55	$^{V}OH–Y^{2+Z}Al^{Z}Al…^{X}\square$
3561.2(1)	26.2	29.96	$^{V}OH–Y^{2+Z}Al^{Z}Al…^{X}Na$
3584.7(2)	11.7(5)	2.51	$^{V}OH–^{Y}Li^{Z}Al^{Z}Al…^{X}\square$
3597.5(1)	20.1(3)	21.17	$^{V}OH–^{Y}Li^{Z}Al^{Z}Al…^{X}Na$
3615.4(7)	10	0.29	$^{V}OH–^{Y}Li^{Z}Al^{Z}Al…^{X}Ca$
3625(1)	18	0.98	$^{W}OH–^{Y}Al^{Y}Al^{Y}Li…^{X}\square$
			$^{W}OH–^{Y}AlY^{2+}Y^{2+}…^{X}\square$
3643(2)	25(3)	0.88	$^{W}OH–^{Y}Al^{Y}Al^{Y}Li…^{X}Na$
3671.9(4)	16	0.95	$^{W}OH–^{Y}AlY^{2+}Y^{2+}…^{X}Na$
3683.5(6)	14	0.52	$^{W}OH–^{Y}AlY^{2+Y}Li…^{X}Na$
3697.8(8)	16	0.39	$^{W}OH–Y^{2+}Y^{2+}Y^{2+}…^{X}Na$
3715.5(6)	20	0.62	$^{W}OH–^{Y}Al^{Y}Li^{Y}Li…^{X}Na$
3737.6(8)	44.1	0.30	$^{W}OH–^{Y}Al^{Y}Li^{Y}Li…^{X}Ca$ (?)
3764.5(8)	45.1	0.30	$^{W}OH– Y^{2+}Y^{2+Y}Li…^{X}Ca$ (?)

FWHM - full width at half maximum. Data in parentheses are standard deviations. The lack of such data at peak position or FWHM denotes that the parameters were fixed.

Fig.1.

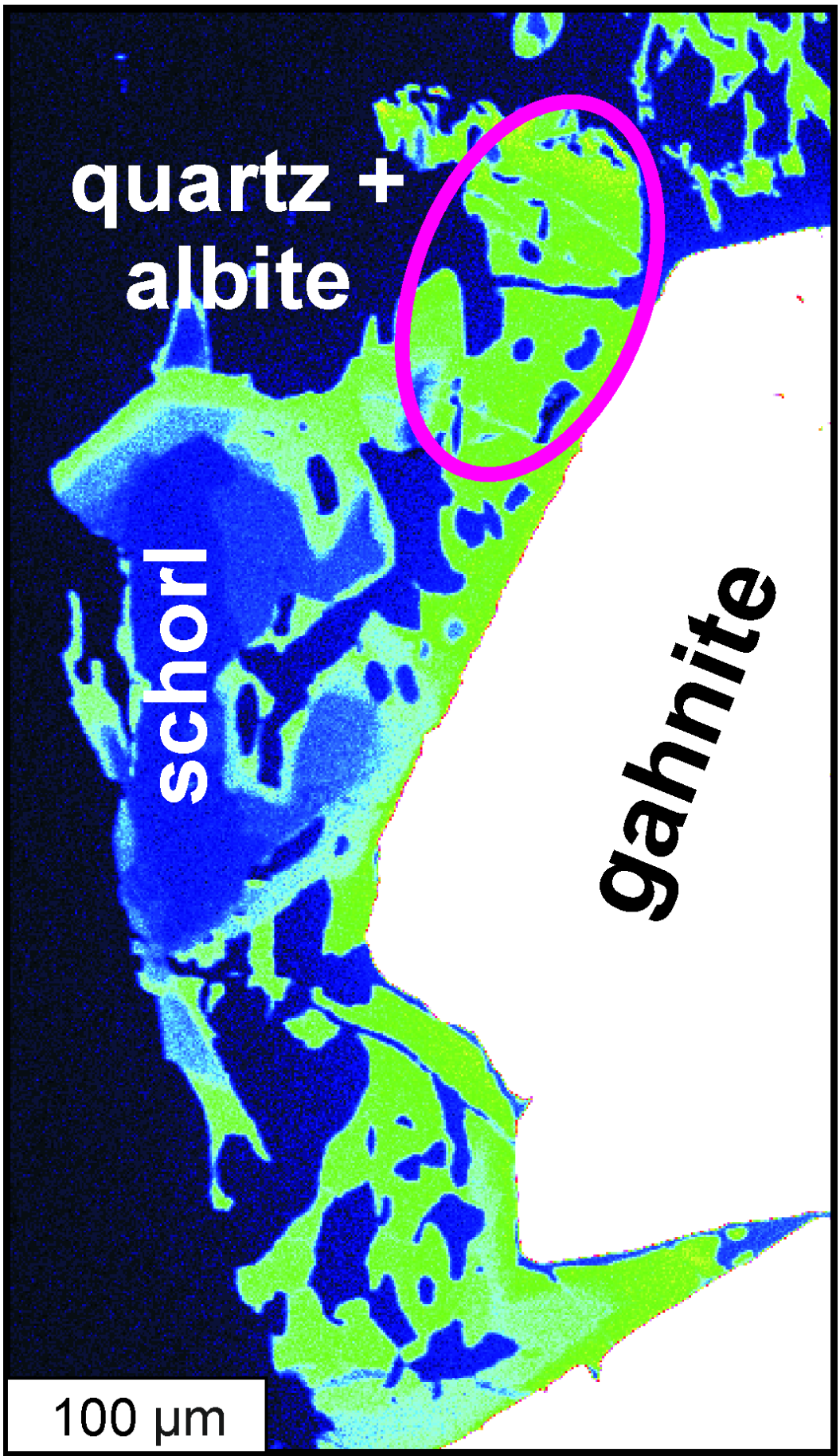

Fig. 2.

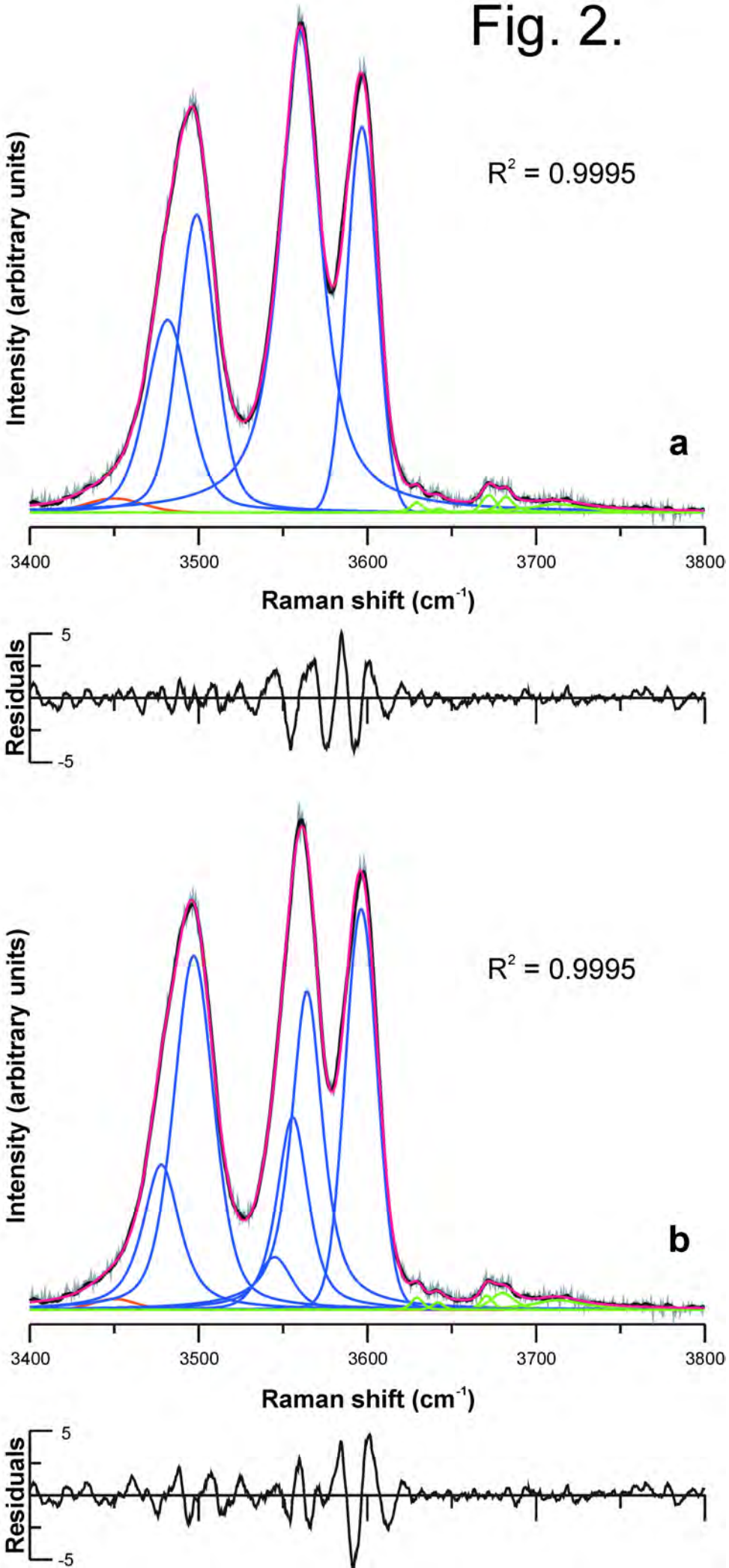
Intensity (arbitrary units)
R^2 = 0.9995
a
3400
3500
3600
3700
3800
Raman shift (cm^{-1})
Residuals
5
-5
Intensity (arbitrary units)
R^2 = 0.9995
b
3400
3500
3600
3700
3800
Raman shift (cm^{-1})
Residuals
5
-5

Fig. 3.

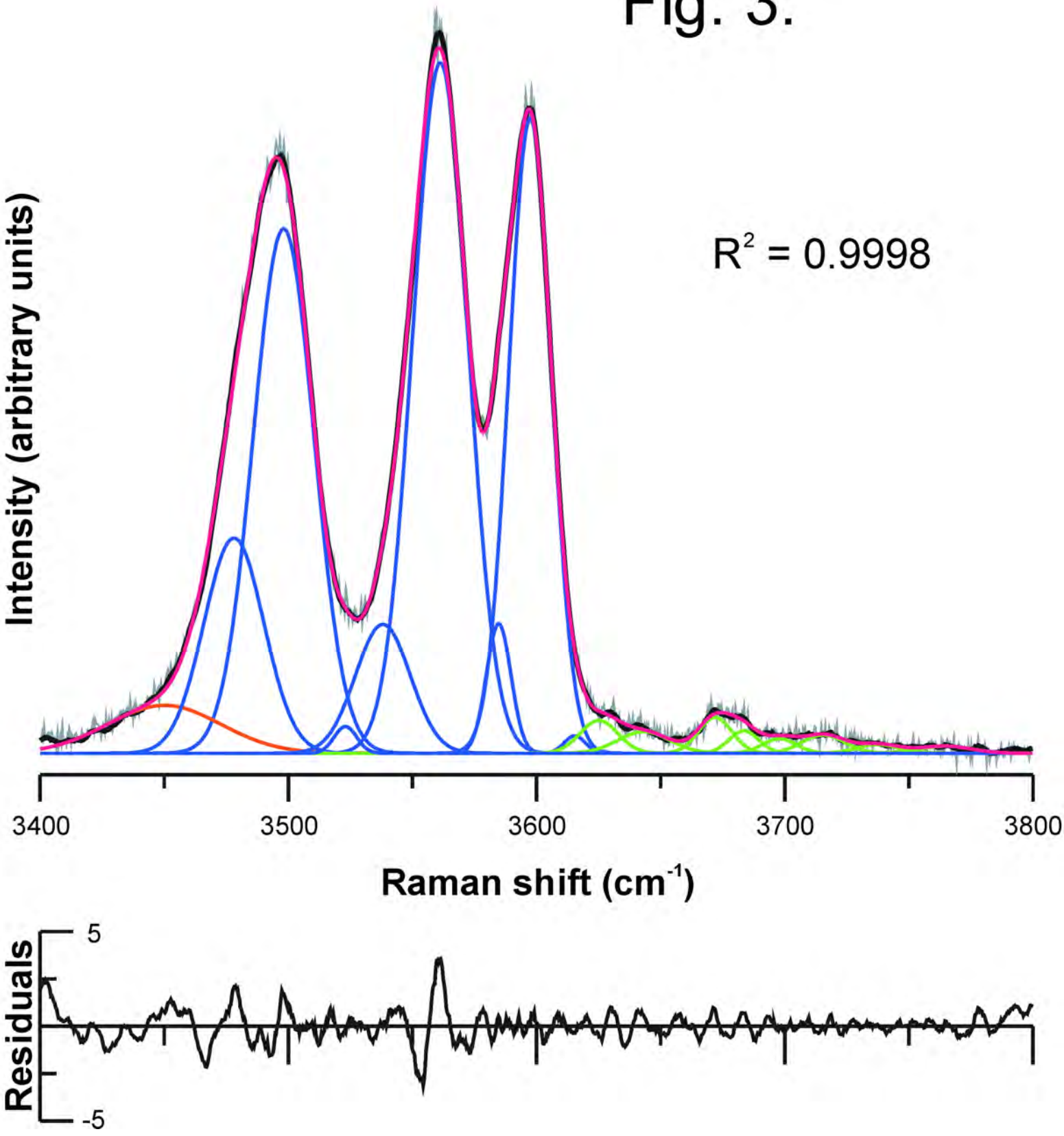
Intensity (arbitrary units)
R^2 = 0.9998
3400
3500
3600
3700
3800
Raman shift (cm^{-1})
Residuals
5
-5